Sveriges lantbruksuniversitet
Swedish University of Agricultural Sciences

Department of Forest Resource Management

Modeling of Effective Leaf Area Index

Modellering av "Effective Leaf Area Index" med fjärranalysdata

Lina Selin

Master Thesis project • 60 credits

SY001 Jägmästarprogrammet

Arbetsrapport / Sveriges lantbruksuniversitet, Institutionen för skoglig resurshushållning, 507 • ISSN 1401-1204

Umeå 2019

Modeling of Effective Leaf Area Index

Modellering av "Effective Leaf Area Index" med fjärranalysdata

Lina Selin

Supervisor:	Persson Henrik, Swedish University of Agricultural Sciences, Department of Forest Resource Management
Assistant supervisor:	Lindberg Eva, University of Agricultural Sciences, Department of Forest Resource Management
Examiner:	Fransson Johan, Swedish University of Agricultural Sciences, Department of Forest Resource Management

Credits:	60 credits
Level:	Second cycle, A2E
Course title:	Självständigt arbete i skogsvetenskap, A2E - Jägmästarprogrammet 60,0 hp
Course code:	EX0922
Programme/education:	SY001 Jägmästarprogrammet
Course coordinating department:	Department of Forest Resource Management
Place of publication:	Umeå
Year of publication:	2019
Title of series:	Arbetsrapport / Sveriges lantbruksuniversitet, Institutionen för skoglig resurshushållning
Part number:	507
ISSN:	1401-1204
Online publication:	https://stud.epsilon.slu.se
Keywords:	Sentinel-1, tree species, random forest, linear discriminant analysis, classification

Abstract

Mapping of effective leaf area index (LAI_e) over the Swedish boreal forest test site Krycklan (64°N19°E) was performed using ground-based field estimates of LAI_e and remote sensing data sources. The LAI_e data were collected 2017 and 2018 using the LAI-2200 Plant Canopy Analyzer and its later version LAI-2200C Plant Canopy Analyzer. The remote sensing data used were airborne laser scanning (ALS) data, Interferometric Synthetic Aperture Radar (InSAR) data from TanDEM-X, and stereo matched drone images. The stereo matched drone images only covered a small subset of the Krycklan catchment, the ICOS grid area. Point cloud metrics were calculated from the ALS data and the drone data such as height percentiles, intensity percentiles, point cloud density and cover metrics. Three metrics from the TanDEM-X data were evaluated as predictors; interferometric phase height, coherence and backscatter. Estimations were done by fitting regression models of LAI_e and the predicting remote sensing data sources. The best ALS regression model for predicting LAI_e used the canopy density gap metric, giving an R^2_{adj}=0.93 for catchment level estimations and R^2_{adj}=0.97 for the ICOS grid area. The TanDEM-X metric interferometric phase height was the single best predictor of the three InSAR metrics, predicting LAI_e with a R^2_{adj}=0.85 at catchment level and R^2_{adj}=0.93 at the ICOS grid area. The drone data model included the variables canopy cover gap and the 99th height percentile, which resulted in a R^2_{adj} value of 0.95. The models were used to generate wall-to-wall rasters and evaluated with the leave-one-out cross validation method. It was concluded that the ALS model was best suited to predict LAI_e as it was able to handle varying forestation, which both the other methods struggled with. When applied over mature and homogeneous boreal forest all models performed with similar accuracy.

Contents

1 Introduction

Diagnosing the environmental health is of high relevance in mapping climate change. A factor that affects all life on this planet from the small scale to a tremendously large scale is photosynthesis. Photosynthesis is a process that occurs inside the chloroplasts of leaf tissue that uses carbon dioxide, water and sunlight to create carbohydrates and oxygen. Approximately 40% of the plant's dry mass consists of carbon that is fixed in photosynthesis and this process enables life on Earth (Lambers, Chapin, and Pons, 2008). The tree canopy is thus an important factor in the ecosystem processes because it affects the energy, carbon and water budgets in an area (Sellers et al., 1997). The canopy leaf area is the dominant controlling factor over primary production, energy exchange, transpiration and other physiological ecosystem attributes (Asner, Scurlock, and Hicke, 2003).

In research of ecological attributes and interactions the Leaf Area Index (LAI) is often used as a measure of the canopy leaf area. LAI describes the density of tree canopy foliage and can be defined as the total one-sided area of leaf tissue per unit ground surface area (Watson, 1947). A model of LAI can be applied on studies that concerns vegetation and ecology and for validation of research. LAI is thus an important factor to consider in monitoring of global atmosphere and biosphere interactions, and the remote sensing arena offers effective methods to do so (Turner et al., 2003). By finding relationships between remote sensing data metrics and field estimates of LAI it is possible to predict corresponding properties over large areas using the area method (Harrie, 2012). The most accurate LAI estimates are given by destructive sampling data which are rarely performed due to high costs and impracticality (Chason, Baldocchi, and Huston, 1991). Common ground-based derivations include the Tracing Radiation and Architecture of Canopies (TRAC) (Homolová et al., 2007), hemispherical images (Manninen et al., 2009) and the LAI-2200C Plant Canopy Analyzer (Eklundh, Harrie, and Kuusk, 2001). The TRAC instrument measures the effect of the spatial distribution of foliage in LAI measurements (Chen, Rich, et al., 1997). The LAI-2200C Plant Canopy Analyzer instrument and its precursors from LI-COR Biosciences, is an optical instrument that measures LAI by assuming that the radiation in the wavelength band 320-490 nm is absorbed by foliage. The measurements made by this instrument are estimates commonly called effective leaf area index (LAI_e), or "plant area index" and differs from LAI because LAI_e includes the areas of branches and stems and assumes that the leaves and needles are randomly distributed in the canopy space (LI-COR, 2013). In reality leaves and especially needles are grouped within shoots. It is shown that instruments that assume a random spatial distribution of leaves and needles often underestimates LAI in boreal forests. This also holds for hemispherical images (Chen, Rich, et al., 1997). The reason is that LAI_e is related to gap fraction and when the biomass is clumped the canopy gap fraction increases (Stenberg, 1996). Like most other ground-based indirect estimations of

LAI the measurements made with LAI-2200C Plant Canopy Analyzer is based on the application of Beer-Lambert law (LI-COR, 2012), an equation that explains the attenuation of light based on the physical properties of the material passed through (Saleh and Teich, 2019).

Previously, LAI has been predicted using LAI_e measurements collected with the Plant Canopy Analyzer from LI-COR and remote sensing data derived from both passive sensors (Chen and Cihlar, 1996; Eklundh, Harrie, and Kuusk, 2001; Kovacs et al., 2004; Manninen et al., 2009; Tillack et al., 2014) and active sensors (Ilangakoon, Gorsevski, and Milas, 2015; Solberg, 2010; Solberg et al., 2009; Sumnall et al., 2016; Tang et al., 2014). In the last decade especially airborne lidar remote sensing has been used in the area, likely due to its ability to capture vegetation structure with high resolution, its possibility to capture large areas and the increasing availability of data. Many studies developed empirical relationships with statistical analysis, mostly regression, between predictor variables derived from lidar metrics and ground-based LAI estimations with promising results; R^2 = 0.85 (Tang et al., 2014), R^2 = 0.67-0.76 (Sumnall et al., 2016). Solberg et al. (2009) evaluated airborne laser scanning (ALS) data in mapping of LAI_e in a Norway spruce forest by fitting regression models of LAI_e against the calculated log-transformed inverse of the ALS penetration rate metric. Two different optical instruments were used for collecting ground-based LAI_e data, the LAI-2000 Plant Canopy Analyzer and hemispherical images (HI). LAI_e based on HI showed a weaker relationship with the ALS data compared to the LAI-2000 Plant Canopy Analyzer, which generated R^2 values above 0.9. This study became a foundation in the forthcoming modeling. Solberg (2010) tested different ALS canopy penetration metrics for their ability in mapping gap fraction, leaf area index and defoliation in a Scots pine forest. The study included the metrics penetration rate and intensity calculated by either first echo or first and last echo. The conclusion was that all four penetration metrics were highly related to field-measured gap fraction and LAI_e measured with the LAI-2000 Plant Canopy Analyzer. However, first and last echoes metrics produced penetration rates closest to the gap fraction and were able to penetrate smaller gaps in the tree crowns.

Other remote sensing techniques have been tested in predicting LAI using ground-based estimations. Manninen et al. (2009) estimated LAI in boreal forest by relating field measured LAI_e from hemispherical images and the LAI-2000 Plant Canopy Analyzer to aerial images taken during wintertime. The R^2 value of the linear regression was 0.89. Chen and Cihlar (1996) used vegetation indices from Landsat TM images together with measurements from the LAI-2000 Plant Canopy Analyzer and the TRAC instrument to estimate LAI and LAI_e in boreal coniferous forest. It was found that spring Landsat images were better than summer images in determining overstory LAI in boreal forests. It was also found that LAI_e was better related to the simple ratio (SR) and normalized difference vegetation index (NDVI) than LAI. The study stated that LAI_e is easier to measure and less variable than LAI, and because it is an intrinsic attribute of plant canopies it was suggested to use LAI_e as the most important parameter for radiation interception considerations. Kovacs et al. (2004) estimated LAI_e in a mangrove forest with IKONOS images using the vegetation indices and measurements from the LAI-2000 Plant Canopy Analyzer. The regression analyses of the LAI_e estimates and the vegetation indices NDVI and SR showed significant relationships of R^2 values slightly above 0.7. Eklundh, Harrie, and Kuusk (2001) compared observed reflectances from the Landsat ETM+ sensor with LAI_e estimates from the LAI-2000 Plant Canopy Analyzer to find statistical relationships. It was shown that the visible wavelength bands were most sensitive to changes in LAI_e. Tillack

et al. (2014) investigated the seasonal relationship between field-measured LAI_e from the LAI-2200 Plant Canopy Analyzer and high resolution satellite-derived vegetation indices. It was concluded that the relationship between LAI_e and spectral vegetation indices varies over the year. Ilangakoon, Gorsevski, and Milas (2015) estimated LAI using terrestrial laser scanning data and measurements from the LAI-2200 Plant Canopy Analyzer and found correlation values between 0.5 and 0.99 for different methods. Few studies have investigated how to predict LAI using a large quantity of ground-based estimates of LAI_e. Moreover, radar data and stereo matched aerial images are rarely used in remote sensing modeling of LAI_e.

The aim of this study was to compare raster predictions of LAI_e developed from three different remote sensing techniques. The statistical models were developed using ground-based LAI_e measurements together with airborne laser scanning (ALS) data, Interferometric Synthetic Aperture Radar (InSAR) data from TerraSAR-X add-on for Digital Elevation Measurement (TanDEM-X) and point clouds from stereo matched aerial images captured from a drone platform. The purpose of the analysis was to shed light on weaknesses and strengths of the three different remote sensing techniques in predicting LAI_e. "The global synthesis of plant canopy LAI", a compilation of over 1000 published estimates world wide presented by Asner, Scurlock, and Hicke (2003) was used as a reference for typical LAI values in boreal forests. According to the Global synthesis of plant canopy leaf area index the mean value of LAI in boreal evergreen needleleaf forests was 3.5. This value was calculated from 94 observations measured with destructive harvesting and direct determination of one-sided leaf area, collection and weighting of leaf litterfall, allometry, indirect contact methods and indirect non-contact methods. To the latter belongs LAI-2200C Plant Canopy Analyzer and its precursors. The maximum LAI value in boreal forests, after removal of statistical outliers according to the Global synthesis of plant canopy leaf area index was 6.2.

2 Material and methods

2.1 The study area

The study covers the area of Krycklan catchment, a research site located 50 km west of Umeå in the vicinity of Vindeln (64°14′N, 19°46′E) in northern Sweden (Figure 2.1). The land ownership of the research site is spread over multiple estates belonging to private land owners and forest companies. Forest covers 87% of the catchment area and the rest consists of mires, rock outcrops and thin soils. The land use is dominated by forestry, and approximately 25% of the catchment has been protected since 1922. Arable land covers 2% of the land area. The dominant tree species are Norway spruce (*Picea abies* (L.) Karst) and Scots pine (*Pinus sylvestris* L.) with smaller quantities of birch (*Betula pendula* Roth.), aspen (*Populus tremula* L.) and contorta pine (*Pinus contorta*). The area is hilly with an elevation varying between 136-373 m above sea level. The forest is overall second growth with a clear-cut area covering a total of 7% between the years 1999–2010 (Laudon et al., 2013).

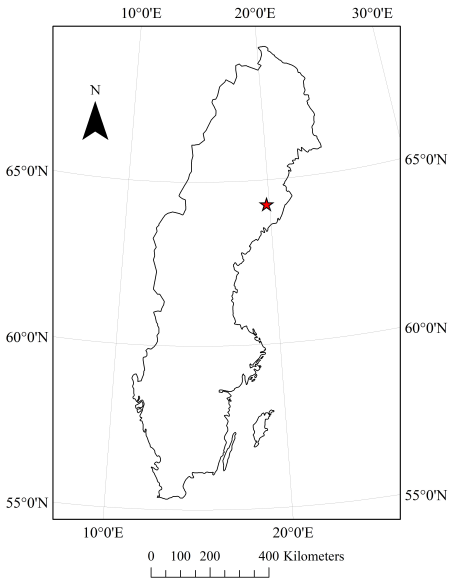

Figure 2.1. The Krycklan catchment is located in northern Sweden (64°N 19 °E) in the municipality of Vindeln.

Two grids of permanent field plots are spread across the catchment (Figure 2.2). One large grid of field plots, containing 436 plots was inventoried 2014 and 2015. The circular field plots with a radius of 10 m are distributed systematically in a square grid with 350 m spacing between adjacent plots over the 6790 hectare area. For every plot, coordinates, forest and vegetation variables are registered. An Integrated Carbon Observation System (ICOS) tower used to track carbon and atmospheric fluxes is located at the site, which is surrounded by a denser grid of field plots (Figures 2.2 and 2.3). The denser ICOS grid is located inside the large grid and was established during the fall of 2016 complementing the large grid with 52 new plots resulting in a grid of 75 field plots with a 10 m radius and 175 m spacing. The inventory contributes with additional survey data of vegetation and plot coordinates (Wallerman et al., 2018).

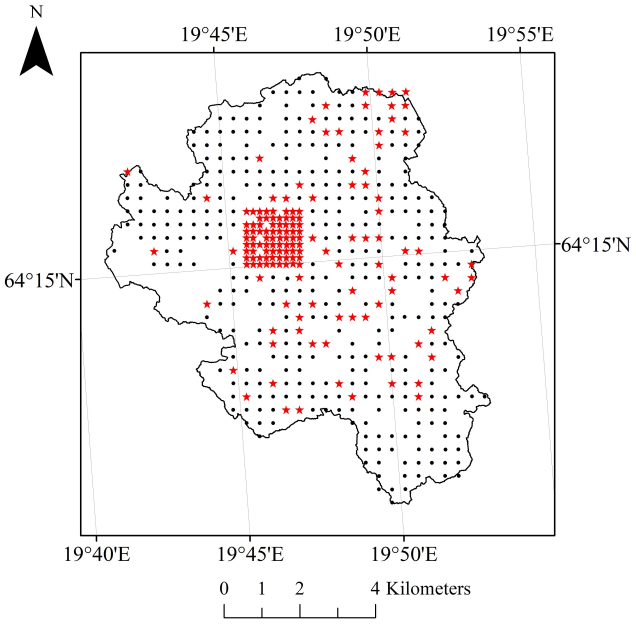

Figure 2.2. Krycklan catchment with the large field plot grid covering the entire catchment and the ICOS grid, a dense grid around the ICOS tower. Red stars = LAI_e measured plots.

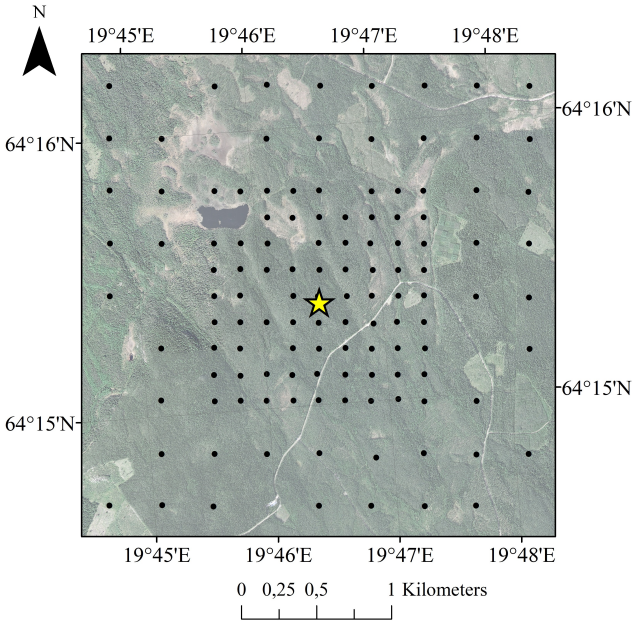

Figure 2.3. The ICOS grid with the ICOS tower in center (yellow star).

2.2 Field data

LAI_e data were collected during the vegetation seasons of 2017 and 2018. In 2017, 25 plots were measured between September 2-7, then an additional set of 128 plots were collected the next summer between June 21 and July 15 to complete the data sample. Time difference in season between the surveys could affect the analysis due to decreasing primary production between July and September (Begon, 2006). Since all the 2017 year's inventoried field plots are dominated by coniferous trees, leaf shedding between the surveys will not be an important issue.

The selection of new sample plots aimed at capturing the variation of forest in the area. Dominating tree species at the field plots inventoried 2014 and 2015 were assumed to be an important factor when deciding which plots to include in the sample to obtain a model that would be able to predict LAI_e for all the forest stands in the catchment. The measurements inventoried 2017 were used together with forest attribute data to find a suitable distribution of sample plots for further collection of LAI_e measurements in 2018. Several regressions models were generated, with the Heureka system, a software developed within the program of Forest Sustainability Analysis (Wikström et al., 2011), to evaluate the relationship between LAI_e and various forest attributes. The strongest correlation was found between branch biomass and LAI_e. Branch biomass refers to the dry biomass of living branches, including leaves and needles (Marklund, 1987, 1988). In the data acquired for analysis, the variable was presented as biomass in ton per hectare. Therefore, the aim was to select plots so that the entire variation of branch biomass for every dominating tree species would be covered in the field data (Figures 2.4 and 2.5). Every plot dominated by a tree species

other than pine or spruce was included in the sample, but since pine and spruce are the two absolutely dominating tree species in the area the whole variation of branch biomass for the other species, such as aspen, was impossible to cover. Aspen was present as the dominating tree species at only two plots in the entire catchment.

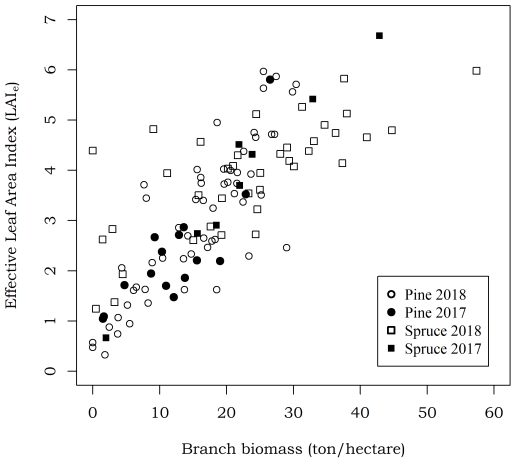

Figure 2.4. LAI_e measurements plotted against branch biomass. Pine and spruce dominated plots measured 2017 (filled symbols) and 2018 (unfilled symbols).

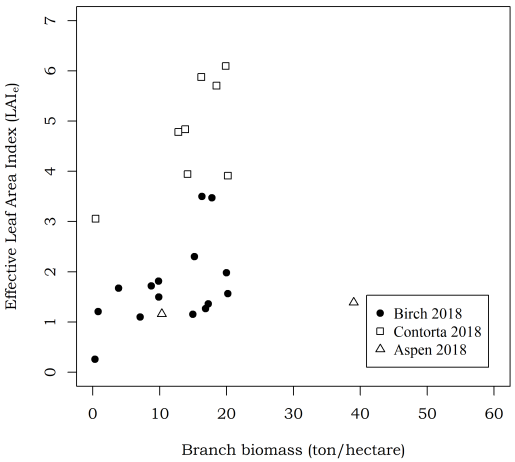

Figure 2.5. LAI_e measurements plotted against branch biomass. Plots dominated by birch (points), contorta pine (squares) and aspen (triangles) measured 2018.

The LAI_e data were collected with the LAI-2200 Plant Canopy Analyzer instrument from LI-COR Biosciences during the vegetation season of 2017 and with the upgraded version LAI-2200C Plant Canopy Analyzer in the summer of 2018. Two sensors were used during the data collection. One reference sensor mounted on a tripod and placed in an open area above ground vegetation level took measurements with close time intervals of 30 seconds. This ensured that the gross amount of radiation in the blue spectrum (320-490 nm) was known. These measurements are further on referred to as above-measurements, because they measure the radiation above the canopy level. The other sensor was brought to the plots to take measurements under the canopy level, below-measurements. Since the blue radiation was assumed to be absorbed by foliage the ratio between below- and above-measurements represents the below canopy transmittance, which is used to calculate LAI_e. The optical sensor of the instrument measures radiation with five concentric sensor rings centered at zenith angles 68°, 53°, 38°, 23° and 7° (Figure 2.6), with the possibility to exclude rings in the post-processing. The instruments were synchronized and calibrated according to the accompanying instruction manual (LI-COR, 2012). Five measurements were taken at each plot, one in the center and four in the ordinal directions (Figure 2.7).

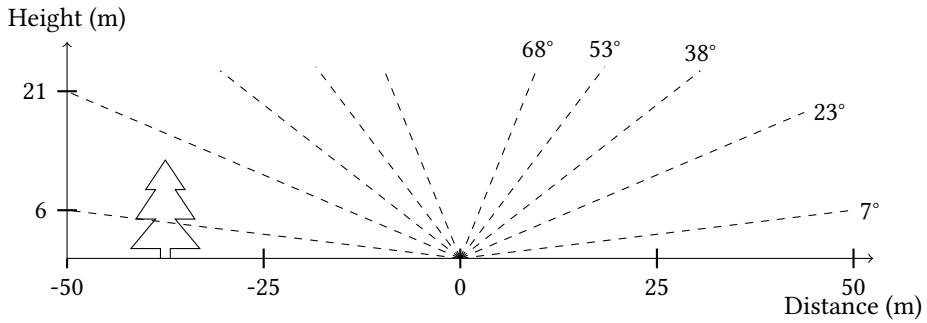

Figure 2.6. The LAI-2200C Plant Canopy Analyzer sensor range with five sensor rings with different zenith angles. Including the 5th ring, at 50 m distance trees above 6 m height will affect the measured LAI_e value.

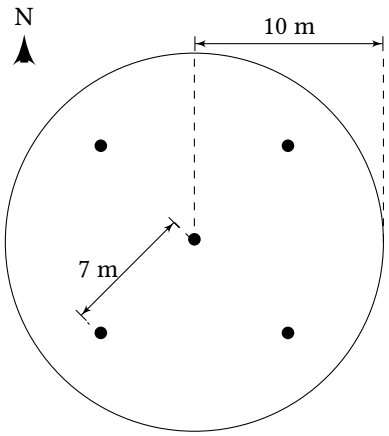

Figure 2.7. Arrangement of measurement within plot.

The field inventories were overall performed in the same way both years, with some exceptions.

2017: Sunset was selected as the optimal sky condition for taking the measurements. 25 plots were measured.

2018: Most of the data collection was done during days with suitable weather conditions with clear blue sky or even cloud cover. The uneven cloud conditions some days were handled by keeping the reference sensor close to ensure that both sensors faced the same sky. 128 plots were measured.

2017: Measurements were taken with the sensor always facing north and using a 180° lens cap to avoid shading from the person holding the instrument (for both above and below sensors).

2018: Measurements were collected with the direct sunlight blocked out using a 90° lens cap, which also blocks out shading from the person holding the instrument (for both above and below sensors).

2017: A calibrated reference sensor for above-measurements was located facing north in an open canopy area larger than 75×75 m^2 and programmed for auto logging every minute at hip height, approximately 1 m above ground.

2018: A calibrated reference sensor for above-measurements was located in an open canopy area larger than 75×75 m^2 and programmed for auto logging every 30 second above field vegetation level, around 1.5 m above ground. The 90° lens cap made it necessary to go back and change the position of the sensor every hour as the sun incidence angle varied.

2.2.1 Definitions

A number of LAI definitions commonly used can be identified (Asner, Scurlock, and Hicke, 2003; Zheng and Moskal, 2009):

1. Total LAI: total one-sided area of photosynthetic tissue per unit ground surface area. Based on the outside area of leaves taking into account the leaf shape.
2. True LAI: one half of the total green leaf area per unit horizontal ground surface area. This is a quantitative method.
3. Inclined projected LAI or silhouette LAI: projected area of leaves while accounting for leaf inclinations.
4. Horizontally projected LAI: area of the shadow that would be cast by each leaf in the canopy with a light source placed perpendicular to it.
5. Effective LAI: one half of the total area of light intercepted by leaves per unit horizontal ground surface area. This definition assumes a random spatial distribution of foliage.

Number two to five are all relatively common in publications concerning LAI. As stated earlier, definition number five was used in this study.

2.3 Remote sensing data

The ALS and the InSAR data in this study covered the Krycklan catchment wall-to-wall, while the stereo matched drone images covered the ICOS grid area.

Time differences between collection of field data and the remote sensing data might affect the models. The field data were collected one to three years after the remote sensing data acquisitions, which means that vegetation growth has occurred and possibly silvicultural treatments. Most forest stands at the Krycklan catchment are dominated by mature coniferous trees and since vegetation growth in mature forest is low the difference in canopy cover will be small. Any silvicultural treatments performed between field data collection and remote sensing data acquisition will appear in the data as outliers.

2.3.1 ALS data

ALS data over Krycklan were collected on 22 and 23 August 2015 by TerraTec Sweden AB. Further specifications can be found in Table 2.1. As the data were collected in August it is assumed that no leaf shedding had occured yet.

Table 2.1. ALS sensor and flight specifications

Date of acquisition	August 22-23, 2015
Platform	FW (Fixed Wing)
Sensor	Titan, serie number L349
Date of calibration	2015-08-01
Flying altitude (m)	987-1123
Flying speed (km/h)	135
Pulse repetition frequency (kHz)	300
Scan angle (°)	35
Mean pulse density (m^{-2})	20
Wavelength (nm)	1064

2.3.2 TanDEM-X data

TanDEM-X data were collected covering the catchment 18 October 2015. Images were attained in strip-map mode with horizontal transmit and horizontal receive (HH) polarization. The mean height of ambiguity (HOA) was 61 m and the scene center incidence angle was 41°. The concept of TanDEM-X is two satellites orbiting the Earth in a close formation cooperating in sending and receiving signals. Unlike when a single operating satellite orbiting the same area observing changes in the landscape over time, acquisitions from two satellites with slightly different locations sending and receiving signals at the same time, are preferred when analyzing forest canopy structures (Persson, 2016).

2.3.3 Stereo matched drone images

Aerial photography was carried out in September 2016 in the area over the ICOS grid. A drone, a four-rotor helicopter equipped with a Parrot SEQUOIA multispectral camera was used. The area was mapped by ten adjacent flying blocks, rectangles measuring 160×800 m^2 oriented north-to-south with the ICOS tower in the center.

The flying altitude was set to 170 m above the launching point, but over the tower the flying height was slightly exceeded. Each block was photographed using 6 to 7 parallel north-to-south flying paths, approximately 35 m apart. The sensor was set to use a very high stereo overlap, 80% along and 80% across flight lines for later production of a dense point cloud from image matching. At the time of data acquisition the deciduous tree species were in different stages of color transformation, but had not shedded leaves yet (Wallerman et al., 2018). Further specifications can be found in Table 2.2.

Table 2.2. Drone sensor and flight specifications

Date of acquisition	September 14 & 19, 2016
Platform	Unmanned Aerial Vehicle (UAV)
Sensor	Sequoia (3.98 mm)
Coordinate system	SWEREF99 TM (EPSG: 3006)
Ground resolution (cm/pixel)	13.9 cm/pixel
Focal lenght (mm)	3.98
Flying altitude (m)	170
Number of images	9504
Bands	3
Coverage area (km^{-2})	3.85
Points	8 210 470
Rotation angles	Yaw, Pitch, Roll
RMS reprojection error	0.228206 (0.52638 pix)
Max reprojection error	3.65271 (26.1361 pix)

2.4 Data Processing

All data were handled in the SWEREF99TM coordinate system, the national geographical reference system. The analysis were made using RStudio, version 1.1.447 (RStudio Team, 2015).

2.4.1 Field data processing

Studies have shown that optical instruments that measures radiation transmittance (gap fraction) and uses inversion models which assumes random spatial distribution of leaves tend to underestimate LAI in boreal forest due to the overlap or clumping of needles on shoots. The LAI-2200C Plant Canopy Analyzer and its precursors belong to this group of instruments and for that reason, the LAI_e values measured in plots dominated by coniferous trees were corrected with clumping index corresponding to the dominating tree species at the plot, estimated with the TRAC instrument by Homolová et al. (2007), Smolander, Stenberg, and Linder (1994) and Jensen et al. (2008).

The assumption that the radiation is absorbed by foliage should sometimes be set aside to correct for the radiation that is reflected and transmitted by the foliage. This so called scattering error is problematic especially when measurements are taken in direct sun light. Corrections could also be made for data measured in obscured sun adjusting for actual foliage scattering properties in the canopy instead of assuming that reflectance and transmittance are both zero. Since all of the measurements

collected 2018 were taken during day time, scattering corrections were made for this data by applying a model by Kobayashi et al. (2013) in the FV2200 program (version 2.1.1, a software accompanying the instrument) according to the FV2200 manual (LI-COR, 2013). The scattering correction includes information about sky conditions, size of sensor lens cap and sensor angles that depends on the sun angles. Measurements collected 2017 were taken during sunset avoiding direct sunlight, thus scatter corrections were not required for that data (Gil, 2018).

The raw data files collected with LAI-2200C instrument were processed in the FV2200 program and a LAI_e value for each plot was calculated from the five LAI_e measurements. Further post-processing methods were used. Primarily, two alternative ways of pairing the above- and below-measurements, interpolated and closest in time LAI_e. Closest in time means that the FV2200 software pairs above-values with below-values that are measured with the least difference in time. The interpolation method were calculated with interpolation of the measurements over time. Closest in time values and interpolated values were post-processed in three additional ways, resulting in a total of eight alternative types of LAI_e.

In Table 2.3 the eight alternative methods for calculating LAI_e and its standard deviation is presented. LAI_e means that the measurements were not processed in any further way and as a default setting the software excluded measurement with high transmittance above a certain threshold. The measurements inventoried 2017 were included in this group, while the three other versions of LAI_e were calculated without 2017 years data due to lack of raw data files.

SMP5 means that all five measurements in each plot were included in the calculations ignoring the high transmittance threshold. 4 rings means that the 5th sensor ring was excluded in the calculations, a setting proposed by Solberg et al. (2009) and illustrated in Figure 2.6.

Of the 128 plots measured 2018, LAI_e could not be calculated by the FV2000 program for nine plots. This was because of non-existing gap values that could be a consequence of no forest vegetation resulting in a high transmittance. It could also be a result of error in the data. The Plant Canopy Analyzer is a highly sensitive instrument responding to small changes in the atmosphere above the sensors. It is realistic to get calculated LAI_e values even at a clear-cut area (though it's a small value) because of nature conservation trees at the site and the wide sensor angle. For the nine plots the forest attribute data from the surveys 2014 and 2015 indicates that trees should be present at the sites, and with these considerations in mind the plots were excluded from the analysis. Of the 25 plots measured 2017, two plots were missing field attribute data for their respective GPS position and both were therefore excluded in the analysis. This means that a total of 142 plots were used in the modeling of LAI_e.

In deciding which LAI_e version to use, a small standard deviation was desired. Low variation in the dependent variable was assumed to give the most robust model, hence the interpolated LAI_e was chosen for further analysis and modeling.

Table 2.3. The different LAI_e were calculated and the standard deviation for these. Number of field plots included are presented in parenthesis (excluding the nine No data plots)

	LAI_e	SMP5	4 rings	SMP5 + 4 rings
Sample size	*(142)*	*(119)*	*(119)*	*(119)*
Closest in time	1.54	1.84	1.96	1.95
Interpolated	**1.52**	1.80	1.94	1.91

2.4.2 ALS data processing

A normalized point cloud was processed using Lastools (Isenburg, 2014). Metrics were extracted from a circle around the plot center. Since the LAI-2200 sensor and the ALS did not capture the same canopy volume (LAI-2200 measures an upwards facing cone whilst the ALS measurements rather corresponds to a downwards facing cone), the circle size to extract metrics from was not obvious. Solberg et al. (2009) tested different circle sizes, static and proportional to tree height and came to the conclusion that 0.75 times the tree height was the best option. To confirm this the same procedure was carried out with the ALS data and the same conclusion was made. Hence, the same radius was used as in Solberg et al. (2009). Mean tree height was estimated by calculating the height percentile p99 in a circle around each plot center with 10 m radius. Metrics such as height percentiles (p05, p10,... p99) and intensity percentiles (int10, int25,... int100), canopy density, canopy cover and the inverse 'gap' of the last two were calculated from the p99-radius sized plots. The canopy cover gap metric was calculated as:

$$P = \frac{R_{\mathrm{g}}}{R_{\mathrm{t}}} \tag{2.1}$$

where R_g is the number of first returns on the ground (under the height cutoff at 1.5 m) and R_t is the total number of first returns, below and above the cutoff. Higher values of P implies less canopy cover. The canopy density gap metric was calculated as:

$$D = \frac{R_{\mathrm{gA}}}{R_{\mathrm{tA}}} \tag{2.2}$$

where R_{gA} is the number of all returns on the ground (under the height cutoff at 1.5 m) and R_{tA} is the total number of all returns, below and above the cutoff. Higher values of D implies less canopy density.

The calculated density gap metric had very few values close to zero compared to the cover gap metric (Figure 2.8). This could indicate that the density metric would be more detailed in it's description of green foliage.

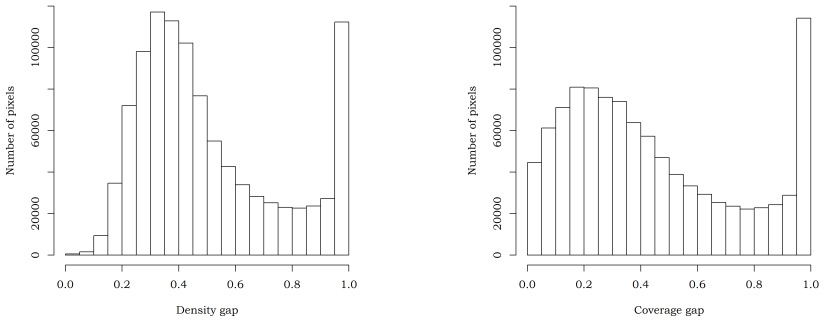

(a) ALS density gap **(b)** ALS cover gap

Figure 2.8. Histograms of raster values calculated from different ALS metrics.

2.4.3 TanDEM-X data processing

The data were delivered in the format of co-registered single-look slant range complex images. The single-look complex data from each TanDEM-X satellite were multilooked with a factor of 5 × 5 looks. The single-look complex resolution was 2.5 m in slant range and 3.3 m in azimuth with a pixel size of 1.36 m and 1.84 m, respectively.

From the TanDEM-X data image pairs the metrics interferometric phase height (φ), and coherence (γ) were calculated with the help of an interferogram, a complex image describing the complex coherence $\widetilde{\gamma}$ as:

$$\widetilde{\gamma} = \frac{E[s_1 s_2^*]}{\sqrt{E[|s_1|^2]E[|s_2^*|^2]}} \tag{2.3}$$

where s_1 and s_2 are the two complex images, one from each satellite, E is the expectation value and * is the complex conjugate, which means taking the phase with opposite sign in order to get the phase difference between the two images. Interferometric phase height is calculated as the argument of the complex coherence, arg($\widetilde{\gamma}$), and coherence is the magnitude of the complex coherence, $|\widetilde{\gamma}|$. One more metric, the backscatter coefficient (σ°) was calculated from the image pair by subtracting the calibration gain provided in the metadata from the multilooked intensity images and then a radiometric normalization was applied. One backscatter image was computed as the arithmetic mean of the two normalized backscatter images.

The processed interferometric phase height, coherence and backscatter rasters were resampled onto an ALS DTM grid with 10 × 10 m^2 pixels. The geocoding was done using a lookup table, generated from cross-correlation between a multilooked intensity image from one of the satellites and a simulated SAR intensity image produced from the ALS DTM (Persson et al., 2017).

For each of the three TanDEM-X metric rasters (interferometric phase height φ, interferometric coherence γ and backscatter σ°) pixel data were extracted around the field plot centers. In order to receive stable data two different ways of extracting values from the rasters were tested. First the bilinear method was used to extract interpolated values from the four nearest raster cells. Then the data were extracted with a circular buffer of 30 m, calculating a mean value of all the pixel cells with the cell center on the border of or within the buffer distance. The data generated with the 30 m buffer yielded slightly better result when modeling LAI_e, likely a result of filtering local extreme pixel values and a better fit to the LAI-2200 sensor optics.

2.4.4 Drone data processing

The drone data processing followed a procedure similar to the ALS data processing, but delimited to the area covering the ICOS grid. The same metrics were calculated. To investigate the properties of the point cloud and its possibility to capture variations in the tree canopy, different radius and height cutoff values were evaluated when calculating the metrics used for the regression modeling.

When calculating the density metric using the drone image point cloud the results are the same as the canopy cover metric. The reason for this is that the point cloud cannot penetrate the canopy to measure density and therefore only the canopy cover metric was evaluated for the drone model.

2.5 Statistical modeling

Solberg et al. (2009) found a strong relationship between LAI_e and ALS penetration rate. Futhermore, they showed that ALS-based LAI_e modeling were advantageously done with a non-intercept logarithmic model. Using the Beer-Lambert law they established the following model:

$$LAI_e = \beta \cdot ln(P^{-1}) + \epsilon \tag{2.4}$$

where β is a slope parameter to be estimated, P is the canopy cover gap metric and ϵ is the error. In the study two different versions of the penetration rate metric were calculated. The first version was based on the first ALS return and the second version was based on the first and the last ALS return. Despite similar R^2 (0.93 and 0.92, respectively) the second version proved to be somewhat more sensitive to variations in near-vertical gap fraction, hence they assumed this penetration rate was more appropriate. With this knowledge in mind, the metrics canopy cover gap and density gap were transformed as per Equation 2.4. For the remaining metrics no transformation of the data were necessary as they all appeared, and was assumed, to have a linear relationship to LAI_e.

The metrics calculated from the point clouds (ALS and drone data) and extracted from the TanDEM-X rasters for each field plot were modeled with linear regression. Several regression models were generated to evaluate various combinations of the calculated metrics. The models generated were based on the generic non-intercept model with one or two predictors:

$$LAI_e = \beta_1 \cdot X_1 + \beta_2 \cdot ln(X_2) + \epsilon \tag{2.5}$$

where β_i are slope parameters to be estimated, X_i are the calculated metrics and ϵ is the error. The Student's t-test was used for evaluating the significance level of each model's parameter estimate β_i. The significance of the models parameter estimates were evaluated using analysis of variance (Table 2.4).

Due to the relatively sparse amount of sample data (142 plots in total, 71 in the ICOS grid area) the models were evaluated with the leave-one-out cross validation method. This means that one single observation were used as validation data while all other observations worked as training data. The procedure was repeated until all observation had been left out, one at a time (Wong, 2015). The resulting cross-validated root mean square error ($RMSE_{cv}$), the cross-validated mean absolute error ($Bias_{cv}$) and the adjusted coefficient of determination (R^2_{adj}) of the models were presented as accuracy indicators of the models.

As the drone data only covers the ICOS grid area, these field plots were used to make additional models for ALS and TanDEM-X as well. This makes the later comparisons of the different methods easier. The comparisons made in this way were comprised of the $RMSE_{cv}$, the $Bias_{cv}$ and the R^2_{adj}.

The development of LAI_e rasters with 10×10 m^2 pixels were done by applying the prediction models to rasters of the calculated metrics. To avoid calculating the logarithm of zero a constant was added to the models. For the ALS and drone data model a constant of 0.1 was chosen empirically and added in the transformation.

Table 2.4. Analyses of variance for the models describing the relationships between remote sensing data and LAI_e. DF = degrees of freedom, SS = sum of squares, MS = mean square, F = Fisher's test and Pr>F = the probability of having a larger F-value by coincidence

Source	Parameter	DF	SS	MS	F	Pr>F
ALS	D	1	1649.39	1649.39	2007.3	< 0.001
	ϵ	141	115.86	0.86		
TanDEM-X	φ	1	1500.91	1500.91	800.6	< 0.001
	ϵ	141	264.34	1.87		
Drone data	P	1	920.21	920.21	1366.08	< 0.001
	$p99$	1	7.97	7.97	11.83	< 0.001
	ϵ	70	47.15	0.67		

3 Results

Five models were created from the different remote sensing data sources, one from drone data and two from both ALS and TanDEM-X. Statistics over the rasters developed from the models are listed in Table 3.1 and the results from the leave-one-out cross validation are presented in Table 3.2.

3.1 ALS

Many metrics showed a significant relationship for estimating LAI_e. Of all the models tested and evaluated the density gap metric was the best predictor of LAI_e, closely followed by the cover gap metric. All of the height (p05, p10,... p99) and intensity metrics (int10, int25,... int100) performed worse than both cover gap and density gap. Therefore, the density gap metric was chosen for further investigation. The best performing model was the fitted non-intercept log-transformed model:

$$LAI_e = -4.42 \cdot ln(D + 0.1) \tag{3.1}$$

where D is the density gap. The predictions, showed in Figure 3.1, showed a tendency of higher variance for lower values of density gap (higher values of the x-axis). It is also possible to distinguish a slight curvature, which results in underestimation of LAI at low density gap levels and overestimation at high density gap levels. It should be noted that a similar curvature was also present for the model using the cover gap metric. There are several outliers that affects the degree of explanation of the model.

The ALS derived LAI_e model predicted a rather homogeneous distribution of LAI_e values around four in the central parts of the catchment corresponding to the ICOS grid area (Figure 3.2). The mean value of the catchment was predicted slightly lower, which is reasonable due to all the non-forest areas. According to the distribution of raster pixel values in the catchment, most pixels were predicted to values around three (Figure 3.3). Hot spot areas with LAI_e values above 7 were spread in the catchment, most commonly in the central and eastern parts. The raster statistics are presented in Table 3.1. Both for catchment and ICOS grid area the model showed good predictions of LAI_e with an adjusted coefficient of determination of R^2_{adj} = 0.93 and R^2_{adj} = 0.97, respectively (Table 3.2).

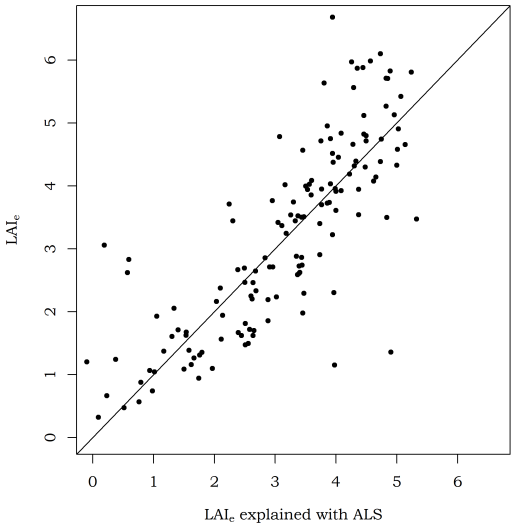

Figure 3.1. LAI_e plotted against the fitted non-intercept ALS model (3.1).

Table 3.1. Statistics for the LAI_e raster predictions developed from ALS, TanDEM-X and drone data. Area 1 = catchment, Area 2 = ICOS grid area

Data Source	Area	Minimum	Maximum	Mean	Standard deviation
ALS	1	-0,42	10.18	2.57	1.78
TanDEM-X	1	-1.76	11.82	2.12	1.57
ALS	2	-0,42	10.18	3.29	1.39
TanDEM-X	2	-1.03	10.69	3.28	1.49
Drone data	2	-0.12	8.57	3.28	1.40

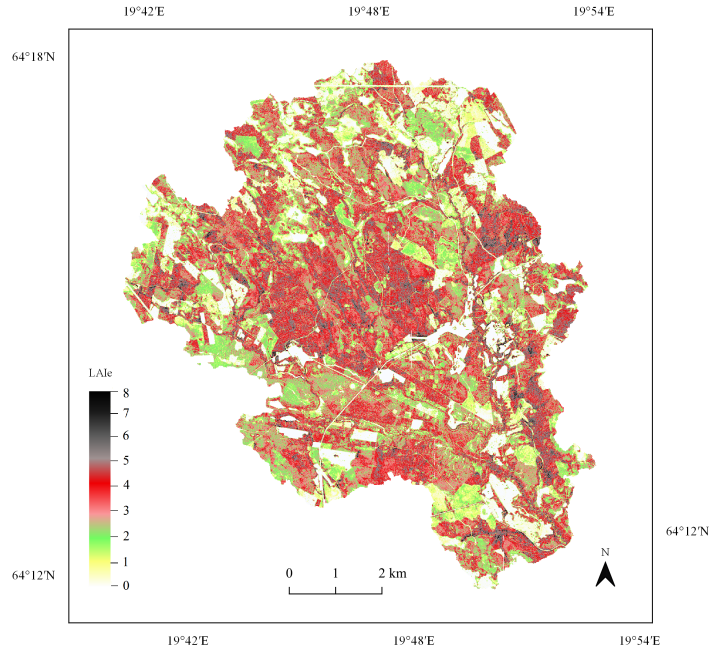

Figure 3.2. A map of LAI_e over Krycklan catchment derived from the ALS model: $LAI_e = -4.42 \cdot ln(D + 0.1)$, with spatial resolution 10×10 m^2.

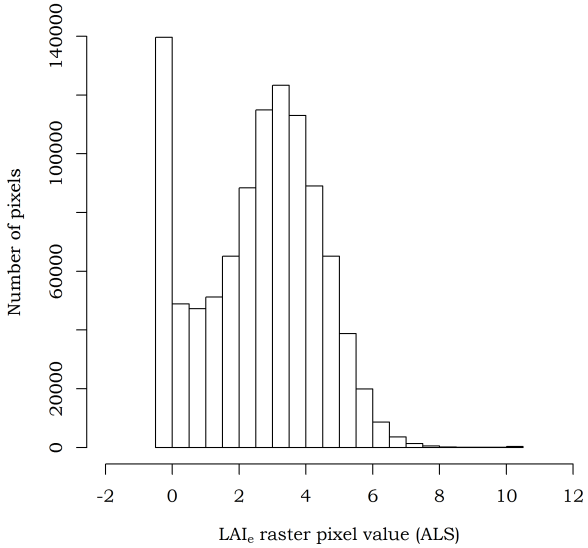

Figure 3.3. The distribution of pixel values in the LAI_e raster created from ALS data.

3.2 TanDEM-X

Values extracted from the phase height raster with 30 m buffer around the field plot center proved to be the most stable method giving the highest correlation to LAI_e. The best model for predicting LAI_e was:

$$LAI_e = 0.37 \cdot \varphi \tag{3.2}$$

where φ is the interferometric phase height. The model showed a high variance with a tendency to higher variance for the underestimated LAI_e compared to the overestimated LAI_e (Figure 3.4). Negative predictions can be derived from negative values in the input phase raster from which phase data were extracted. When creating the LAI_e raster (Figure 3.5) negative pixel values were set to zero.

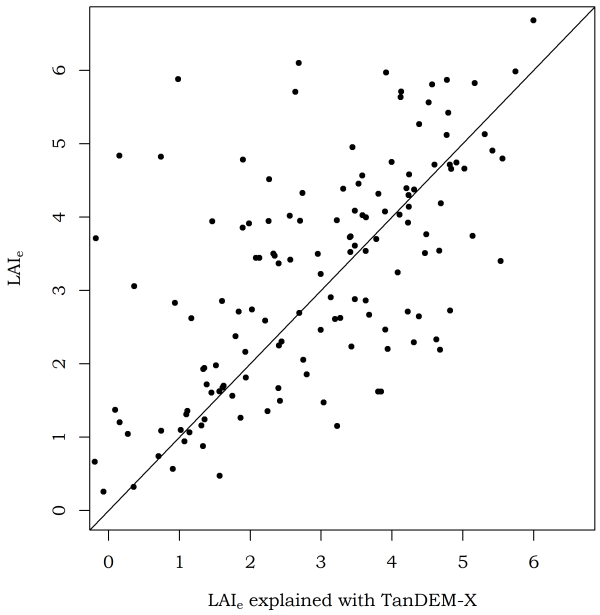

Figure 3.4. LAI_e plotted against the fitted TanDEM-X model (3.2).

The model estimated higher LAI_e values in central parts of the Krycklan catchment with overall lower values in peripheral areas. The minimum pixel value of the TanDEM-X-based LAI_e raster was -1.76, the maximum pixel value was 11,82, the mean pixel value was 2.12 and the standard deviation was 1.57. This is a very large spread and include many unreasonable values of LAI_e. The occurrences of pixel values predicted to LAI_e values between zero and four are equally common in the raster, with a very small quantity of pixels predicted to LAI_e values higher than eight (Figure 3.6). The raster estimations indicate hot spot areas in the central and eastern part of the catchment (Figure 3.5). These hot spots areas coincide with the ones shown in the ALS raster (Figure 3.2). For the catchment and the ICOS grid area the model predicted LAI with an adjusted coefficient of determination of R^2_{adj} = 0.85 and R^2_{adj} = 0.93, respectively (Table 3.2).

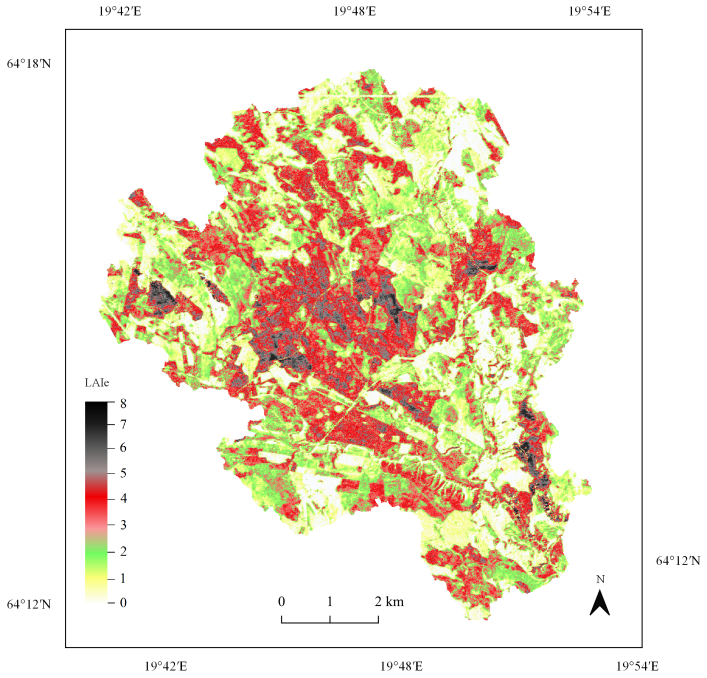

Figure 3.5. A map of LAI_e over Krycklan catchment derived from the TanDEM-X model: $LAI_e = 0.37 \cdot \varphi$, with spatial resolution 10×10 m^2.

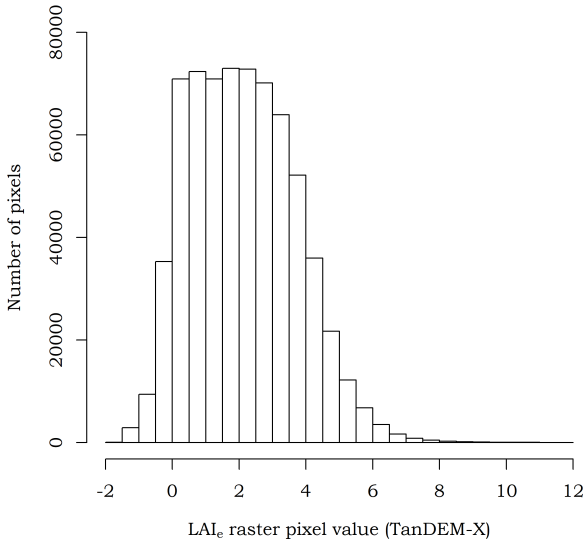

Figure 3.6. The distribution of pixel values in the LAI_e raster created from TanDEM-X data.

3.3 Drone data

When calculating the point cloud metrics a radius of 15 m around the field plot center and 1.5 m height cutoff gave the best result. The two most important explanatory variables in estimating LAI_e with the drone data covering the ICOS grid area were the metrics canopy cover gap and the 99th height percentile, in the model:

$$LAI_e = -1.30 \cdot ln(P + 0.1) + 0.069 \cdot p99 \tag{3.3}$$

where *P* is the canopy cover gap metric and *p99* is the 99th height percentile calculated from the drone data. The data points with values close to zero in the metric cover gap, representing forest with dense tree canopy, were stacked near each other to the right in the plot (Figure 3.7). This phenomenon can be derived from the characteristics of photogrammetry point clouds, which demands a rather large gap in the forest to be able to penetrate the tree canopy.

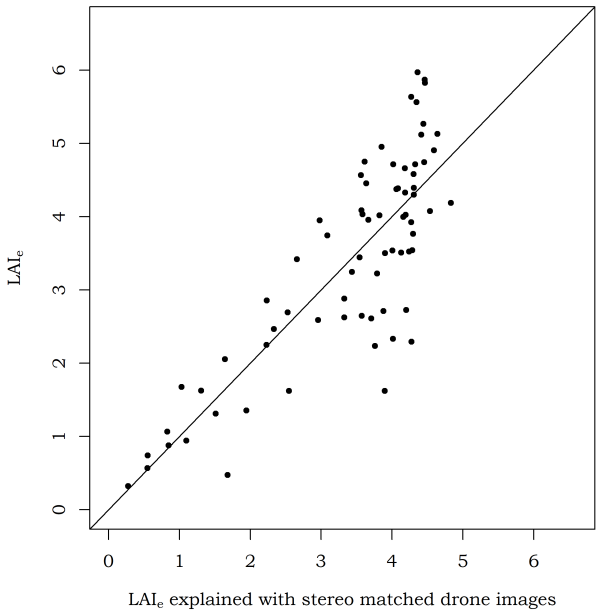

Figure 3.7. LAI_e plotted against the fitted drone data model (3.3).

The raster over the ICOS grid area (Figure 3.8) shows that the majority of the forest was predicted to LAI_e values around four, which is also evident in the pixel value distribution presented in Figure 3.9. A few smaller areas were predicted to pixel values between five and eight along the edges of the ICOS grid area.

The minimum pixel value of the drone data-based LAI_e raster was -0.12, the maximum pixel value was 8.57, the mean pixel value was 3.28 and the standard deviation was 1.40. Statistics for a cut-out of the ICOS grid area from the ALS and TanDEM-X derived raster are presented in Table 3.1. The adjusted coefficient of determination for the drone data model was R^2_{adj} = 0.95 (Table 3.2).

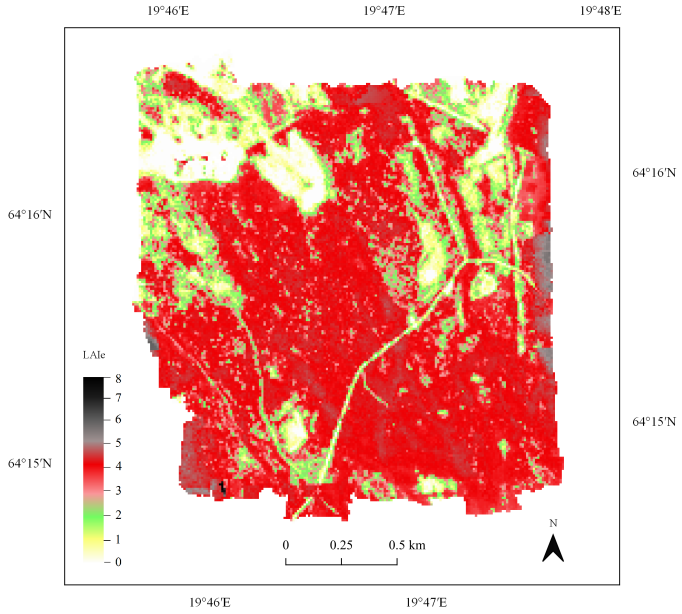

Figure 3.8. A map of LAI_e over ICOS grid area derived from the drone data model: $LAI_e = -1.30 \cdot ln(P + 0.1) + 0.069 \cdot p99$, with spatial resolution 10×10 m^2.

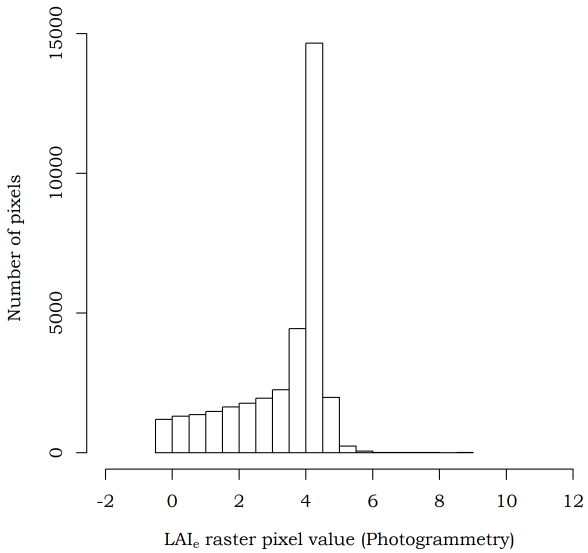

Figure 3.9. The distribution of pixel values in the LAI_e raster created from drone data.

Table 3.2. Estimation of LAI_e from ALS, TanDEM-X and drone data. Area 1 = catchment, Area 2 = ICOS grid area

Data Source	Area	R^2_{adj}	$RMSE_{cv}$	$Bias_{cv}$
ALS	1	0.93	0.91	0.66
TanDEM-X	1	0.85	1.37	0.99
ALS	2	0.97	0.64	0.49
TanDEM-X	2	0.93	1.00	0.79
Drone data	2	0.95	0.83	0.65

4 Discussion

The purpose of this study was to examine the possibility to map LAI_e with three different remote sensing techniques separately; ALS, TanDEM-X and drone-acquired photogrammetry data. The three data sources were all capable of predicting LAI_e with different qualifications and limitations. A limitation concerning all of the models is that they were predicting LAI_e, which differs from LAI and that will affect the application of the model. In cases when LAI is needed it would be necessary to introduce corrections.

The Plant Canopy Analyzer instrument is highly sensitive to exposure and solar illumination condition and the recommendation is to execute data collection under uniform sky; clear blue or even cloud cover, preferably before sunrise or after sunset. The weather conditions were a crucial factor for the collection 2017, resulting in few good days to measure and a small field data set. In the summer of 2018 the priority was rather to collect more data under conditions as good as possible due to time constraints. There was a trade off between quality and quantity. Of all the data points in this study 85% were collected during the summer of 2018. When plotting the predicting variables against LAI_e there was a tendency to increased variance depending on collecting day. This tendency was most evident when plotting LAI_e against the TanDEM-X phase variable, the model with the largest variance. It was data from particularly three days that seemed to cause more variance than other days and that was July 3, 5 and 9, 2018. These days were noted as "Sun and cloud" while most of the other inventory days 2018 were noted as "Clear blue sky" or "Even cloud cover". This observation agrees with the sky test information in the Fv2200 manual (LI-COR, 2013). Variance can be seen in the data from 2017 as well, but then limited to a few data points. This confirms the importance of weather and sky conditions during collection of optical LAI_e data from the Plant Canopy Analyzer instrument and that a more careful selection of days in the field based on the sky conditions would have generated less variance in field data.

The data from 2017 were collected in September whereas the data from 2018 were collected in late June to mid-July. Since the primary production changes over the vegetation season it is possible that the data collected 2017 in average would underestimate LAI_e in comparison to the 2018 years data. This is because the lower gross primary production in the late vegetation season absorbs less blue radiation than earlier during the season. The Plant Canopy Analyzer, which measures LAI_e with the information about the absorbed blue radiation will therefore get lower readings. The ratio between above and below measurements might not be affected by this since the incoming radiation also declines later during the season.

The ALS model shows a high correlation to LAI_e at catchment level (R^2_{adj} = 0.93). This can be explained by the ALS ability to penetrate the canopy, which enabled more precise estimations of the canopy density. The TanDEM-X model estimated LAI_e

over the catchment level with lower correlation (R^2_{adj} = 0.85) compared to the ALS model. The raster statistics (Table 3.1) shows a higher standard deviation in the ALS model compared to the TandDEM-X model. The higher standard deviation in the ALS derived LAI_e raster can be explained by the many pixel values at zero, while the TanDEM-X derived LAI_e raster has a much more even spread (Figures 3.3 and 3.6). The TanDEM-X model had a larger minimum and maximum value spread, which could indicate a more unstable model. Most of the catchment area was predicted with TanDEM-X to LAI_e values below four, but in isolated areas the LAI_e value was predicted extremely high, up to around twelve. Values this high is definitely not reasonable and should be considered a detriment to the model. The mean value of LAI_e was lower for the TanDEM-X model. This in combination with the increased variance for the underestimated values indicates that the model has problem with scarcely forested areas where it underestimates the LAI_e. It would be interesting to further investigate how to improve estimations made on areas with sparse forestation.

The ALS model showed several outliers, which would affect the degree of explanation of the model. An investigation into these field plots could be good in order to possibly exclude any outliers.

Solberg et al. (2009) suggested a logarithmic ALS-based LAI_e model with a penetration rate metric similar to *P*. The calculated density gap metric show overall similar values as cover gap. However, for small values of cover gap, the density is a lot higher. The difference between these metrics are that the canopy density gap includes all ALS returns, while the canopy cover gap includes only first returns. It would not be unreasonable to assume that a metric measuring the density of the tree canopy as opposed to a metric measuring the proportion of the canopy related to the total area, would make for a better estimator of photosynthesizing biomass. The hot spot areas predicted with ALS to LAI_e around seven seemed to coincide with the forest inventory plots dominated by Contorta pine. Contorta pine has a larger proportion of green biomass compared to for example Scots pine. This would further emphasize the importance of the density metric as a Contorta pine stand compared to a Scots pine stand could possibly have similar cover gap metrics, but very different density gap metrics. Further investigations of this would be of interest.

During the LAI_e raster calculations the models had to be able to handle zero values in the input rasters. In order to avoid calculating the logarithm of zero, a constant value was added to the ALS and the drone data model. It was assumed that adding this constant would have little effect on the model's accuracy. For cover and density gap values larger than 0.9 the model returns negative LAI_e values which is not acceptable. Setting the negative values to zero in the resulting raster was assumed to be reasonable, because values above 0.9 excluding the constant factor would have ended up close to zero.

The models developed and cross validated with the ICOS area field plots all showed better predictions compared to their catchment level counterpart. This would indicate that it is easier to predict LAI_e in a mature and homogeneous forest compared to a forest with a more varying degree of forestation. The ALS model performed the best in terms of adjusted coefficient of determination, the cross-validated root mean square error and the cross-validated mean absolute error, followed by the drone data model and last the TanDEM-X (Table 3.2).

The drone data model included the ICOS area, which was covered by forest with less variation in stand mean age and tree volume compared to the whole catchment. A property of photogrammetry point clouds is its similarity to a blanket resting on top of the tree crowns. In a dense forest it cannot easily find the space between

the tree tops and struggles to detect the ground. This differentiates it from the ALS point cloud, which penetrates the canopy better. The spatial distribution of photogrammetry data points are dependent on the image overlap and are a lot more uneven and sparse than ALS point cloud data. A penetration rate variable calculated from a photogrammetric point cloud data will be more rough than the ALS generated variable. Even so, the one single metric that could explain LAI_e the best was the canopy cover gap variable. By including the p99 metric to the logarithmic model, it enabled the model to predict higher values, which is crucial. The cover gap model without an additional metric would have difficulties predicting LAI_e values higher than four. To calculate a photogrammetric point cloud with the ability to penetrate the canopy better would have demanded more images with a more extensive image overlap. That kind of data set would require a lot of data capacity for processing and the points might still not penetrate the tree crown.

The possibility to use a drone to acquire data for LAI_e estimations opens up for new estimations whenever desired and it is more accessible than ALS and TanDEM-X data. It would be of interest for further drone data modeling of LAI_e to include spatial considerations in the modeling, such as looking at how local maximum could help predict gaps in the canopy. This was partly achieved by including the 99th height percentile into the model.

When comparing the methods for estimating LAI_e based on the ICOS grid area one thing stand out. All the models share similar mean values and standard deviations. This would indicate that for mature and homogenous forests all models predict mean LAI_e quite well. The main difference of the models are their ability to predict LAI_e in forests where silvicultural treatments have been made. This is shown in the TanDEM-X's ability to predict the mean of the ICOS grid area well, but having difficulties doing the same for the entire catchment. How the drone data model handles varying forest is difficult to tell by just looking at the ICOS grid area and it would therefore be very interesting to further expand on the drone data to include the entire catchment. As for the performance of the drone data model on the catchment level, the best guess would be that it performs with higher accuracy than TanDEM-X, but with lower accuracy than ALS in a similar fashion as it did over the ICOS grid area.

The mean LAI_e measurements of the ICOS grid area around 3.3 in this study agrees with previous measurements made in boreal forest presented in the Global synthesis of plant canopy leaf area index. This value might give a more representative picture of the forest state than the catchment mean value around 2.5, since the catchment to a greater extent includes pixel values from agricultural areas, mires, roads, clear cut areas and the lake.

5 Conclusions

The three models developed showed how different remote sensing data sources with completely different characteristics can be used together with ground-based field data of LAI_e to create models to predict LAI_e.

The best estimations of LAI_e were predicted by the ALS model, which could explain 93% of the variance at catchment level (R^2_{adj} = 0.93) and 97% (R^2_{adj} = 0.97) at the ICOS grid area. The second best estimation, at the ICOS grid area, was made by using the drone data model, which could explain 95% of the variance (R^2_{adj} = 0.95). The TanDEM-X model (R^2_{adj} = 0.85 at catchment level and R^2_{adj} = 0.93 at the ICOS grid area) showed a higher variance compared to both other models. The model had problem with underestimating LAI_e in non-homogeneous forest. This resulted in a much lower mean value at catchment level.

The canopy density metric showed a closer relationship to LAI_e compared to the canopy cover metric. The canopy density metric can only be calculated using the ALS point cloud, which favors the ALS model over the drone model. As the drone model was developed and applied solely over the ICOS grid area, a homogeneous area with mature coniferous forest, it would be of interest to develop a drone model based on field data and images over a larger area with a more varying degree of forestation.

All methods predicted LAI_e in line with the values presented in the Global synthesis of plant canopy leaf area index for boreal forests. The models were able to predict the mean value of the ICOS grid area well. In applications where the mean of a homogeneous forest is to be predicted, it would seem that all models predict similarly and are therefore interchangeable. For these kinds of applications the most accessible and cost effective remote sensing method can be used.

References

Asner, G., Scurlock, J., and Hicke, J. (2003). "Global synthesis of leaf area index observations: Implications for ecological and remote sensing studies". In: *Global Ecology & Biogeography* 12, pp. 191–205.

Begon, M. (2006). *Ecology : From individuals to ecosystems*. 4. ed. Oxford: Blackwell Publishing. ISBN: 1405111178.

Chason, J. W., Baldocchi, D. D., and Huston, M. A. (1991). "A comparison of direct and indirect methods for estimating forest canopy leaf area". In: *Agricultural and Forest Meteorology* 57.1, pp. 107–128. ISSN: 0168-1923. DOI: https://doi.org/10.1016/0168-1923(91)90081-Z.

Chen, J. and Cihlar, J. (1996). "Retrieving leaf area index of boreal conifer forests using Landsat TM images". In: *Remote Sensing of Environment* 55.2, pp. 153–162.

Chen, J., Rich, P., et al. (1997). "Leaf area index of boreal forests: Theory, techniques, and measurements". In: *Journal of geophysical research*, pp. 29429–29443.

LI-COR (2012). *LAI2200 Plant Canopy Analyzer: Instruction Manual*. 984-10633. Version Rev 2. LI-COR, Inc.

— (2013). *FV2200 User Guide*. Version 2.0 rev.1. LI-COR, Inc. URL: https://www.licor.com/documents/2iyxh17kxzdokn6pjxq3wk6p9cpw3ok1.

Eklundh, L., Harrie, L., and Kuusk, A. (2001). "Investigating relationships between Landsat ETM+ sensor data and leaf area index in boreal conifer forest". In: *Remote Sensing of Environment* 78, pp. 239–251.

Gil, I. A. (2018). *Understory above- and belowground biomass allocation over the growing season and across different boreal forest stands in Northern Sweden - A boreal forest landscape study*. Droevendaalsesteeg 3a (Lumen, Building 100), 6708 PB Wageningen, The Netherlands: Plant Ecology, Nature Conservation Group. Wageningen University, and Research (WUR).

Harrie, L. (2012). *Geografisk informationsbehandling: Teori, metoder och tillämpningar*. Studentlitteratur AB. ISBN: 9789144088778.

Homolová, L. et al. (2007). "Comparison of different ground techniques to map leaf area index of Norway spruce forest canopy". In: *Proceedings 10th International Symposium on Physical Measurements and Spectral Signatures in Remote Sensing (ISPMSRS)*, pp. 499–504.

Ilangakoon, N. T., Gorsevski, P. V., and Milas, A. S. (2015). "Estimating leaf area index by Bayesian linear regression using terrestrial LiDAR, LAI-2200 Plant Canopy Analyzer, and Landsat TM spectral indices". In: *Canadian Journal of Remote Sensing* 41.4, pp. 315–333. DOI: 10.1080/07038992.2015.1102629.

Isenburg, M. (2014). *LAStools-Efficient Tools for LiDAR Processing*. Version 140709, academic. URL: https://rapidlasso.com/lastools/.

Jensen, J. L. et al. (2008). "Discrete return lidar-based prediction of leaf area index in two conifer forests". In: *Remote Sensing of Environment* 112.10, pp. 3947–3957. ISSN: 0034-4257. DOI: 10.1016/j.rse.2008.07.001.

Kobayashi, H. et al. (2013). "On the correct estimation of gap fraction: How to remove scattered radiation in gap fraction measurements?" In: *Agricultural and Forest Meteorology* 174-175, pp. 170–183. ISSN: 0168-1923. DOI: 10.1016/j.agrformet.2013.02.013.

Kovacs, J. M. et al. (2004). "Estimating leaf area index of a degraded mangrove forest using high spatial resolution satellite data". In: *Aquatic Botany* 80.1, pp. 13–22. ISSN: 0304-3770. DOI: https://doi.org/10.1016/j.aquabot.2004.06.001.

Lambers, H., Chapin, F. S., and Pons, T. L. (2008). "Photosynthesis". In: *Plant Physiological Ecology*. New York, NY: Springer New York, pp. 11–99. ISBN: 978-0-387-78341-3. DOI: 10.1007/978-0-387-78341-3_2.

Laudon, H. et al. (2013). "The Krycklan Catchment Study—A flagship infrastructure for hydrology, biogeochemistry, and climate research in the boreal landscape". In: *Water Resources Research* 49.10, pp. 7154–7158. DOI: 10.1002/wrcr.20520.

Manninen, T. et al. (2009). "Leaf Area Index (LAI) estimation of boreal forest using wide optics airborne winter photos". In: *Remote Sensing* 1.4, pp. 1380–1394. ISSN: 2072-4292. DOI: 10.3390/rs1041380.

Marklund, L. (1987). *Biomassafunktioner för gran i Sverige*. Rapport 43. Sveriges lantbruksuniversitet, Institutionen för skogstaxering, p. 127.

— (1988). *Biomassafunktioner för tall, gran och björk i Sverige*. Rapport 45. Sveriges lantbruksuniversitet, Institutionen för skogstaxering, p. 73.

Persson, H. (2016). *Remote sensing of forest. Radar remote sensing of forest*. Skogshushållningsserien. The Swedish University of Agricultural Sciences, Department of Forest Resource Management.

Persson, H. et al. (2017). "Experiences from large-scale forest mapping of Sweden using TanDEM-X data". In: *Remote sensing* 9.1253, pp. 2072–4292.

RStudio Team (2015). *RStudio: Integrated Development Environment for R*. RStudio, Inc. Boston, MA. URL: http://www.rstudio.com/.

Saleh, B. and Teich, M. (2019). *Fundamentals of Photonics*. Wiley Series in Pure and Applied Optics. Wiley. ISBN: 9781118770092. URL: https://books.google.se/books?id=rcqKDwAAQBAJ.

Sellers, P. et al. (1997). "BOREAS in 1997: Experiment overview, scientific results, and future directions". In: *Journal of geophysical research* 102.D24, pp. 28, 731–28, 769.

Smolander, H., Stenberg, P., and Linder, S. (1994). "Dependence of light interception efficiency of Scots pine shoots on structural parameters". In: *Tree Physiology* 14.7-8-9, pp. 971–980. DOI: 10.1093/treephys/14.7-8-9.971.

Solberg, S. (2010). "Mapping gap fraction, LAI and defoliation using various ALS penetration variables". In: *International Journal of Remote Sensing* 31.5, pp. 1227–1244. DOI: 10.1080/01431160903380672.

Solberg, S. et al. (2009). "Mapping LAI in a Norway spruce forest using airborne laser scanning". English. In: *Remote Sensing of Environment* 113.11, pp. 2317–2327. ISSN: 0034-4257. DOI: 10.1016/j.rse.2009.06.010.

Stenberg, P. (1996). "Correcting LAI-2000 estimates for the clumping of needles in shoots of conifers". In: *Agricultural and Forest Meteorology* 79.1, pp. 1–8. ISSN: 0168-1923. DOI: 10.1016/0168-1923(95)02274-0.

Sumnall, M. J. et al. (2016). "Estimating leaf area index at multiple heights within the understorey component of Loblolly pine forests from airborne discrete-return

lidar". English. In: *International Journal of Remote Sensing* 37.1, pp. 78–99. ISSN: 0143-1161. DOI: 10.1080/01431161.2015.1117683.

Tang, H. et al. (2014). "Deriving and validating Leaf Area Index (LAI) at multiple spatial scales through lidar remote sensing: A case study in Sierra National Forest, CA". In: *Remote Sensing of Environment* 143, pp. 131–141. ISSN: 0034-4257. DOI: 10.1016/j.rse.2013.12.007.

Tillack, A. et al. (2014). "Estimation of the seasonal leaf area index in an alluvial forest using high-resolution satellite-based vegetation indices". In: *Remote Sensing of Environment* 141, pp. 52–63. ISSN: 0034-4257. DOI: 10.1016/j.rse.2013.10.018.

Turner, W. et al. (2003). "Remote sensing for biodiversity science and conservation". In: *Trends in Ecology & Evolution* 18.6, pp. 306–314. ISSN: 0169-5347. DOI: https://doi.org/10.1016/S0169-5347(03)00070-3.

Wallerman, J. et al. (2018). *Mapping state of the forests surrounding the ICOS towers at Svartberget, Norunda and Hyltemossa in years 2015 and 2016.*

Watson, D. (1947). "Comparative physiological studies on the growth of field crops: I. Variation in net assimilation rate and leaf area between species and varieties, and within and between years". In: *Annals of Botany* 11.41, pp. 41–76.

Wikström, P. et al. (2011). "The Heureka Forestry Decision Support System: An Overview." In: *MCFNS* 3, pp. 87–95.

Wong, T.-T. (2015). "Performance evaluation of classification algorithms by k-fold and leave-one-out cross validation". In: *Pattern Recognition* 48.9, pp. 2839–2846.

Zheng, G. and Moskal, L. (2009). "Retrieving Leaf Area Index (LAI) using remote sensing: Theories, methods and sensors". In: *Sensors* 9, pp. 2719–2745. ISSN: 1424-8220. DOI: 10.3390/s90402719.